

Active colloidal propulsion over a crystalline surface

PAPER

Udit Choudhury,^{1,2,a} Arthur V. Straube,^{3,a} Peer Fischer,^{1,4} John G. Gibbs,^{1,5,b}
and Felix Höfling^{1,3,6,c}

¹ Max Planck Institute for Intelligent Systems, Heisenbergstr. 3, 70569 Stuttgart, Germany

² University of Groningen, Nijenborgh 4, 9747 AG Groningen, The Netherlands

³ Department of Mathematics and Computer Science, Freie Universität Berlin, Arnimallee 6, 14195 Berlin, Germany

⁴ Institute for Physical Chemistry, University of Stuttgart, Pfaffenwaldring 55, 70569 Stuttgart, Germany

⁵ Department of Physics and Astronomy, Northern Arizona University, Flagstaff, AZ 86011, USA

⁶ Institute for Theoretical Physics IV, University of Stuttgart, Pfaffenwaldring 57, 70569 Stuttgart, Germany

Submitted to: *New. J. Phys.*; Dated: 21 September 2018

Abstract

We study both experimentally and theoretically the dynamics of chemically self-propelled Janus colloids moving atop a two-dimensional crystalline surface. The surface is a hexagonally close-packed monolayer of colloidal particles of the same size as the mobile one. The dynamics of the self-propelled colloid reflects the competition between hindered diffusion due to the periodic surface and enhanced diffusion due to active motion. Which contribution dominates depends on the propulsion strength, which can be systematically tuned by changing the concentration of a chemical fuel. The mean-square displacements obtained from the experiment exhibit enhanced diffusion at long lag times. Our experimental data are consistent with a Langevin model for the effectively two-dimensional translational motion of an active Brownian particle in a periodic potential, combining the confining effects of gravity and the crystalline surface with the free rotational diffusion of the colloid. Approximate analytical predictions are made for the mean-square displacement describing the crossover from free Brownian motion at short times to active diffusion at long times. The results are in semi-quantitative agreement with numerical results of a refined Langevin model that treats translational and rotational degrees of freedom on the same footing.

Keywords: colloidal microswimmers; active Brownian motion; surface diffusion; hexagonal close-packed monolayer

1. Introduction

The non-equilibrium behaviour of active and passive particles ranging from microorganisms such as bacteria and artificial microswimmers to passive colloidal particles is the focus of a large number of ongoing studies [1–4]. Whereas biological microswimmers locomote by means of inherently embedded nanomotors generating wave-like deformations of their bodies or appendages, non-biological active particles must be engineered to support the special conditions to cause self-propulsion. Passive colloidal particles can be navigated by external fields or field gradients and can exhibit nontrivial collective behavior [5–9]. In contrast, active colloidal particles, the focus of our study, propel in a fluid medium also in the absence of the above driving factors; for a review see, e.g.,

^a These two authors contributed equally.

^b Electronic mail: john.gibbs@nau.edu

^c Electronic mail: f.hoeftling@fu-berlin.de

ref. [4]. By consuming fuel or energy, they typically create local field gradients by themselves, leading to self-propulsion, while being subjected to rotational Brownian diffusion [10–14].

The motion of a particle can be significantly affected by the presence of a confining boundary. Due to hydrodynamic coupling, the mobility of a passive particle dragged or rotating in the vicinity of a plane wall is significantly suppressed [15]. In addition, active motion near surfaces [16–23] or other boundaries such as fluid interfaces [24] is complicated by the swimmer–wall interaction depending in general on the detailed properties of the swimmer, the wall, and the fluid [4]. For instance, the concentration of chemical fields near self-phoretic swimmers can be modified by the presence of a surface. Further, active particles tend to accumulate at surfaces, even in the absence of direct, e.g., attractive electrostatic, interactions between the swimmer and the surface [25].

Apart from surfaces, colloidal particles have also been confined by imposing external potentials. The transport properties of passive colloidal particles have recently been shown to change when driven over one- [26–29] and two-dimensional [29–33] spatially periodic potential landscapes. Further complexity arises for time-dependent [34–37] and spatially random potentials [38–42]. Depending on the details of driving mechanism, the use of such landscapes can result in the possibility to precisely control the speed of the net motion [27, 28, 35, 37], the strength of the diffusion [26, 31, 32, 39] and the appearance of transport anomalies [34, 36, 40–42]. For active colloids confined by external potentials, it has been found that, in certain cases, they behave similarly to passive particles with an elevated effective temperature [43, 44] or subject to an effective potential [45]. Initial simulation studies of microswimmers exploring a heterogeneous, random landscape [46, 47] suggest a rich phenomenology due to the interference of the landscape with the persistence properties of the trajectories.

In this combined experimental and theoretical study, we investigate the interplay of active propulsion and a periodic confining potential. Experimentally, active colloidal micro-spheres [11, 48, 49] are moving over a periodic surface realized as a hexagonal close-packed (HCP) monolayer of colloidal particles. The particles’ activity is controlled by changing the concentration of a chemical propellant. Theoretically, the three-dimensional motion of an active colloid over the crystalline surface is treated as active Brownian motion in a two-dimensional energy landscape, while also accounting for the particles’ rotational diffusion. We demonstrate an intricate interplay between confinement effects and active motion, leading to non-trivial dependencies of long-time diffusion coefficients and crossover timescales.

The paper is outlined as follows: in section 2, we describe the experimental system and analysis methods and infer quantitative estimates of model parameters. The aspect of active propulsion over a planar surface is discussed in section 3. In section 4, we proceed to the general case of propulsion over the crystalline surface, which includes the derivation of analytic approximations, the analysis of experimental data, and numerical simulations. We conclude by summarizing our findings in section 5.

2. Experimental system

2.1. Materials and Methods

First we describe the experimental system and how the activity of the particles may be tuned by changing the concentration of a chemical propellant, as shown in several previous reports [10, 11, 50]. A hexagonal close-packed (HCP) monolayer consisting of spherical silica (SiO_2) microbeads (average diameter $d = 2.07\mu\text{m}$ with a coefficient of variation of 10–15%, Bangs Laboratories) forms the periodic surface upon which the active colloids move; the lattice constant of the crystal is set by the particle diameter. The HCP monolayer was prepared with a Langmuir-Blodgett (LB) deposition technique [51] and covered an entire silicon wafer. A scanning electron microscope (SEM) image of the monolayer can be seen in fig. 1(b), and the actual topography of the surface is inferred from the atomic force microscope (AFM) image in fig. 1(d).

The silica microspheres were first functionalized with allyltrimethoxysilane then dispersed in chloroform. This colloidal suspension was then distributed over the air–water interface of an LB trough. A cleaned silicon wafer is dipped into the trough and, upon slowly pulling out the wafer, the

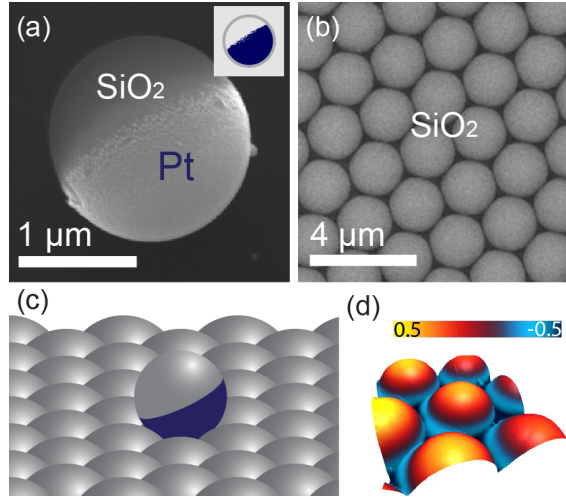


Figure 1. (a) Scanning electron microscope (SEM) image of a single half-coated Janus particle; inset: the dark-blue shows the location of the Pt cap. (b) Top-view SEM image of an HCP monolayer of SiO_2 microbeads. (c) An oblique-view schematic of Janus particle situated on the periodic, two-dimensional lattice, giving a sense of the corrugated, periodic morphology of the surface. (d) Atomic force microscope (AFM) image exhibiting the topography of the surface, color indicates the height in μm .

monolayer is compressed to form a close-packed assembly. This process transfers the monolayer from the air–water interface to the silicon wafer. The wafer is then dried and treated with air plasma to remove any organic impurities before the experiments. While the LB technique yields large area HCP monolayers of silica beads, microscopic line defects can result from the lattice mismatch between adjacent self-assembled colloidal crystals [52]. In order to ensure consistency of the underlying substrate topography, the lattice experiments were carried out on the same piece of wafer by varying the peroxide concentration for the same batch of particles.

The active colloids were fabricated by evaporating a 2 nm Cr adhesion layer followed by 5 nm of Pt onto microbeads of the same type as used for the monolayer; see fig. 1(a) for an SEM image. The thus formed Janus spheres were then suspended into H_2O and subsequently pipetted onto an HCP lattice surface [fig. 1(c)]. The Pt on the Janus particle catalyzes the decomposition of hydrogen peroxide (H_2O_2) and thus gives rise to self-propulsion [11]. The strength of the propulsion was altered by adding different concentrations of aqueous H_2O_2 to the colloidal suspension, covering concentrations between 0 and 6% (v/v). For each concentration, trajectories from 10 randomly chosen Janus particles were recorded for 100 s at a frame rate of 10 fps with a Zeiss AxioPhot microscope in reflection mode with a $20\times$ objective coupled to a CCD camera (pixel size $5.5\,\mu\text{m} \times 5.5\,\mu\text{m}$, resolution 2048×1088).

2.2. Data analysis

We computed time-averaged mean-square displacements (MSDs) of 10 trajectories for each H_2O_2 concentration, and by averaging the MSDs at each lag time we obtain the “averaged MSD” and its standard error. Data fitting was performed with the software OriginLab (OriginLab Corp., Northampton, MA) using a Levenberg–Marquadt iteration algorithm. Due to the linearly spaced time grid, the data points accumulate in the double-logarithmic representation at large times. To account for the different density of data points at short and long lag times on logarithmic scales, we used $1/t$ as weighting factor. The fits were then performed simultaneously for all 10 data sets of each concentration such that the different scatter of the data points enters the error estimate of the fit parameters. The value of the free diffusivity D_0 at different H_2O_2 concentrations was slightly adjusted afterwards to obtain the best match with the averaged MSD curves.

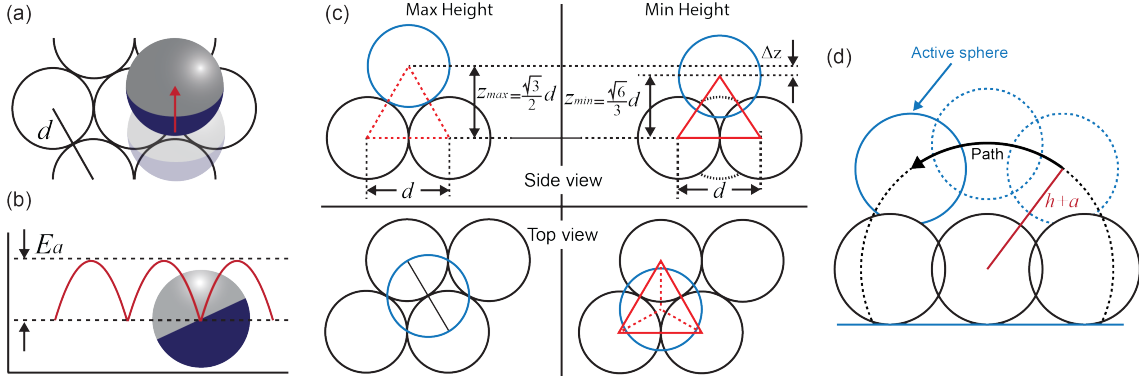


Figure 2. (a) Top-view schematic of a single hop from one potential well to an adjacent one. (b) Side-view schematic of an active particle situated in an energy minimum. (c) Geometry of the barrier between adjacent potential wells due to the HCP lattice substrate. Top row: side-view of the mobile particle (blue circle) at its highest and lowest out-of-plane positions, z_{\max} and z_{\min} on the left and right columns, respectively. Bottom row: corresponding top-views, representing the in-plane positions of the mobile particle with respect to the location of the substrate particles (black circles). (d) A cross-sectional representation of the Janus sphere traversing the energy barrier as it moves from one adsorption site to an adjacent one. The center of the sphere follows the black curved arrow, which is a section of a circle of radius $h + a$, where h is the “elevation” above the crystalline surface. The maximum position corresponds to the dashed light-blue circle in the top-center portion of the figure.

2.3. Height of the potential barrier

Under gravity the Janus particles settle onto the substrate; once settled, Brownian motion leads to effectively two-dimensional diffusion in the gravitational potential imposed by the surface. The potential exhibits a periodic, hexagonal structure of potential wells with adjacent energy minima separated by a distance $d/\sqrt{3}$. A series of “hops” are observed between adjacent energy minima, or in analogy to surface diffusion, adjacent “adsorption sites.” Figure 2(a) schematically demonstrates a single hop from one minimum to an adjacent one. A successful hop requires the Janus particle to overcome an energy barrier of height E_a , as depicted in fig. 2(b).

The gravitational potential $U(\mathbf{x}) = \Delta m g z(\mathbf{x})$ is given by the buoyant mass Δm of the Janus particle, the acceleration g due to gravity, and the height profile $z(\mathbf{x})$ at the two-dimensional position \mathbf{x} . The energy barrier between adjacent potential minima is thus $E_a = \Delta m g \Delta z$, where Δz follows from elementary geometry as shown in fig. 2(c) for the configurations of maximal and minimal height. At the barrier maximum (left column of fig. 2(c)), the centers of two substrate particles and the mobile one form an equilateral triangle. The Janus particle is thus elevated by $z_{\max} = \sqrt{3}d/2$ above the centers of the substrate particles. If the Janus particle is found in a potential minimum, the centers of three substrate particles and the mobile one form a regular tetrahedron, thus $z_{\min} = \sqrt{6}d/3$. For a successful hop, the particles must overcome a geometric barrier of height $\Delta z = z_{\max} - z_{\min} \approx d/20$, which evaluates to $\Delta z \approx 100$ nm for $d = 2$ μm . This is consistent with the surface’s height profile obtained from AFM, see fig. 1(d).

The second ingredient to the energy barrier E_a is the total force on the Janus particle, which results from the competition of gravitation and buoyancy, *i.e.*, the energy barrier is also a function of the material from which the Janus particle is made. Let us first consider a silica sphere which has no metal coating. Then the buoyant mass is $\Delta m = \Delta \rho V_{\text{SiO}_2}$, where $\Delta \rho = \rho_{\text{SiO}_2} - \rho_{\text{H}_2\text{O}}$ is the difference in density between SiO_2 and H_2O , and $V_{\text{SiO}_2} = (4/3)\pi a^3$ is the volume of the fluid displaced by the particle of radius $a = d/2$. For a bare SiO_2 bead of 2 μm diameter, this yields $E_a = 1.7 k_B T$ in terms of thermal energy $k_B T$.

In the case of the Janus particle, the asymmetric distribution of the metallic coating needs to be taken into account. Even though the volume of the cap is small in comparison to that of the bead, it has a significant effect on E_a due to the higher density of Pt. Following ref. 53, we model the

hemispherical cap as ellipsoidal in shape; the thickness Δa of the deposited metal is largest at the top of the sphere and tapers to zero at the equator. This assumption is justified from the deposition process, which delivers the atoms in the vapor plume ballistically to the surface of the sphere. The volume of the cap then reads $V_{\text{Pt}} = [(4/3)\pi a^2(a + \Delta a) - (4/3)\pi a^3]/2 = (2/3)\pi a^2\Delta a$, and with this, the buoyant mass of the Janus particle is $\Delta m = (\varrho_{\text{SiO}_2} - \varrho_{\text{H}_2\text{O}})V_{\text{SiO}_2} + (\varrho_{\text{Pt}} - \varrho_{\text{H}_2\text{O}})V_{\text{Pt}}$. Adopting a value of $\Delta a = 5 \text{ nm}$ as the maximal thickness of the Pt cap and using $\varrho_{\text{Pt}} = 21.4 \text{ g/cm}^3$, we estimate $E_a = \Delta m g \Delta z \approx 2.1 k_B T$ for the energy barrier of the Janus particle.

2.4. Distance of the particle to the surface

For the Janus particle moving passively over a smooth plane, we have measured for the translational diffusion constant $D_0 = 0.13 \text{ } \mu\text{m}^2/\text{s}$, which implies a translational (hereafter indicated by the subscript ‘T’) hydrodynamic friction of $\zeta_T = k_B T / D_0 = 3.2 \times 10^{-8} \text{ Pa s m}$ at $T = 298 \text{ K}$. As expected, the presence of a surface increases the hydrodynamic friction compared to unbounded motion: comparing with the Stokes friction $\zeta_T^{\text{St}} = 6\pi\eta a \approx 1.74 \times 10^{-8} \text{ Pa s m}$ in H_2O ($\eta = 0.89 \text{ mPa s}$), we find $\zeta_T \approx 1.8 \zeta_T^{\text{St}}$. For a planar surface, the friction coefficient ζ_T of a sphere of radius a dragged parallel to the surface at a distance h from the sphere center obeys Faxén’s famous result [15, 54]:

$$\frac{\zeta_T^{\text{St}}}{\zeta_T} \simeq 1 - \frac{9}{16} \frac{a}{h} + \frac{1}{8} \left(\frac{a}{h}\right)^3 - \frac{45}{256} \left(\frac{a}{h}\right)^4 - \frac{1}{16} \left(\frac{a}{h}\right)^5, \quad a \ll h, \quad (1)$$

Inserting the above experimental value for ζ_T and solving for h with $a = 1 \text{ } \mu\text{m}$, we obtain $h \approx 1.3 \text{ } \mu\text{m}$ leaving a gap of $h - a \approx 0.3 \text{ } \mu\text{m}$ between the two surfaces of the Janus particle and the planar substrate.

Note that Faxén’s calculation relies on a far-field expansion of the flow field and is justified only for small ratios a/h . As can be seen *a posteriori* we have $a/h \approx 0.8$, implying slow convergence. Indeed, truncating after the 3rd order in a/h yields an unphysical $h < a$, which is fixed by the 4th order term. The 5th order term yields merely a relative correction of 2%, which suggests convergence of the series. In the following, we anticipate that the translational friction ζ_T does not change appreciably for the range of H_2O_2 concentrations used, although it may be modified for active motion due to altered boundary conditions at the colloid’s surface [21].

3. Active motion on a plane and enhanced diffusion

In order to control the activity, we exploit the H_2O_2 -concentration dependence of active motion seen in catalytic chemical self-propulsion [11]. On a flat, planar surface, the MSD after a lag time t is given by [11]

$$\Delta R_{\text{a,p}}^2(t) = 4 \left(D_0 + \frac{1}{2} v^2 \tau_{\text{rot}} \right) t + 2 v^2 \tau_{\text{rot}}^2 (e^{-t/\tau_{\text{rot}}} - 1), \quad (2)$$

which follows upon assuming independence of translational diffusion of the colloid center and rotational diffusion of the Pt cap orientation; here D_0 is the diffusion coefficient for passive Brownian motion over a smooth plane, v the root-mean-square propulsion velocity in the plane, and τ_{rot} the persistence time of the propulsion direction. The subscripts ‘a’, ‘0’ are used to distinguish between the *active* and *passive* motion and ‘p’ refers to the case of *planar* surface. Qualitatively, eq. (2) implies that the active colloid undergoes passive diffusion for $t \ll \tau_0 := 4D_0/v^2$, ballistic motion for $\tau_0 \ll t \ll \tau_{\text{rot}}$, and enhanced diffusion for $t \gg \tau_{\text{rot}}$. In the latter regime, the MSD grows linearly with time with an increased diffusion coefficient $D_{\text{a,p}} = D_0 + v^2 \tau_{\text{rot}}/2$. Thus at long times, the motion of the active particle displays an enhanced diffusion relative to the motion of the passive particle ($v = 0$).

Figure 3 shows the experimental results for active motion on a smooth, planar surface for the six H_2O_2 concentrations investigated, from which the enhanced diffusion was obtained. The solid curves in fig. 3 are fits to eq. (2), following the procedure in section 2.2, with the obtained parameters given in table I. In the inset of fig. 3, we have rectified the MSD by dividing by the time lag t . This way, the crossover from Brownian diffusion D_0 at short times to enhanced diffusion

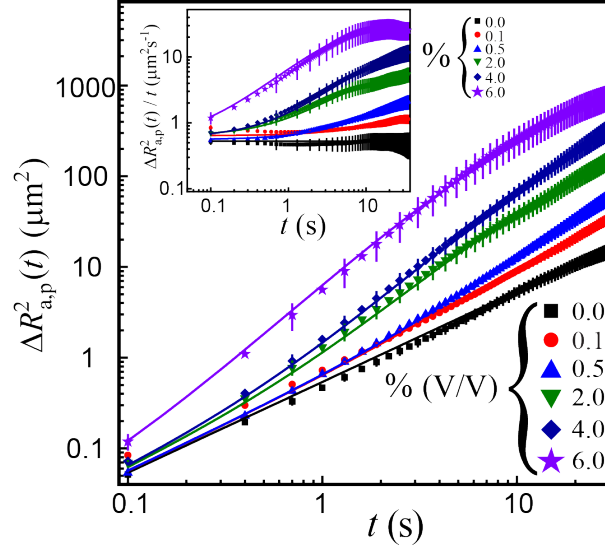


Figure 3. Experimental MSDs of the active particles moving over a planar surface for six H_2O_2 concentrations (v%/v). Solid lines are fits to eq. (2). Inset: rectification plot of the same data showing $\Delta R_{a,p}^2(t)/t$ vs. t in order to more clearly expose the crossover from Brownian to enhanced diffusion. It also serves as a test of the fit quality.

c (%(v/v))	D_0 ($\mu\text{m}^2/\text{s}$)	$D_{a,p}$ ($\mu\text{m}^2/\text{s}$)	τ_{rot} (s)	v ($\mu\text{m}/\text{s}$)
0	0.13	0.13 ± 0.05	—	0
0.1	0.16	0.35 ± 0.06	11 ± 3	0.18 ± 0.01
0.5	0.14	0.7 ± 0.2	12 ± 3	0.30 ± 0.01
2	0.16	1.4 ± 0.5	4.2 ± 0.7	0.77 ± 0.04
4	0.15	3.6 ± 0.8	7.9 ± 1.2	0.93 ± 0.04
6	0.14	8.0 ± 1.6	2.3 ± 0.6	2.6 ± 0.3

Table I. Parameters obtained from fitting eq. (2) to the MSD data for active motion atop a planar substrate, shown in fig. 3. The long-time diffusion coefficient $D_{a,p}$ was calculated from $D_{a,p} = D_0 + v^2 \tau_{\text{rot}}/2$. The uncertainties are standard errors of the mean obtained from the fitting procedure.

$D_{a,p}$ at long times can be inferred more easily, and this representation serves also as a sensitive test of the fit quality.

The short-time diffusivity D_0 was varied between $0.14 \mu\text{m}^2/\text{s}$ and $0.18 \mu\text{m}^2/\text{s}$ to obtain the best match with the averaged MSD curves. The small variability of the background diffusivity may be attributed to the sparseness of data points at short timescales, but it may also reflect possibly altered boundary conditions at the surface due to the catalytic reaction. We have found that the propulsion velocity v measured this way (table I) increases monotonically with the H_2O_2 concentration c . Similarly, the long-time diffusivity $D_{a,p}$ grows progressively with the increase in c and is enhanced over D_0 for all concentrations $c > 0$ studied, in accordance with eq. (2). We remark that v and $D_{a,p}$ for $c = 6\%$ (v/v) are significantly larger than the corresponding values for $c = 4\%$ (v/v), suggesting that additional effects become important for the propulsion mechanism at this high concentration. Finally, we observe a large, non-monotonic variation of τ_{rot} , signifying that the rotational motion is non-trivially altered by the activity. We attribute this to imperfections in the Janus particle, causing deviations from axisymmetric symmetry and thus the possibility of a residual active angular velocity on the particle.

4. Active motion atop a crystalline surface

4.1. Theory

The behavior of the active colloids moving across the crystalline surface is significantly different from the planar case. The catalyzed chemical reaction on the Pt side leads to two effects described first qualitatively: (i) similar to the planar case, the Janus particles are actively and directionally propelled over the surface away from the catalyst coating [55]. (ii) In contrast to the planar case, motion over the crystalline surface is hindered by the particle becoming transiently trapped within potential wells.

According to the above reasoning, the active Brownian motion in the periodic potential $U(\mathbf{x})$ may be modelled in a simplified way by an over-damped Langevin equation:

$$\dot{\mathbf{x}}(t) = \mathbf{v}(t) - \zeta_T^{-1} \nabla U(\mathbf{x}(t)) + \sqrt{2D_0} \boldsymbol{\xi}_T(t). \quad (3)$$

Here, $\mathbf{x}(t)$ and $\mathbf{v}(t)$ are, respectively, the vectors of the particle position and of the propulsion velocity projected onto the plane of the crystalline surface. The latter is incorporated via the second term on the right hand side of eq. (3). Further, $\boldsymbol{\xi}_T(t)$ is a two-dimensional Gaussian white noise of zero mean and unit (co-)variance, $\langle \boldsymbol{\xi}_T(t) \otimes \boldsymbol{\xi}_T(s) \rangle = \mathbf{I} \delta(t-s)$ with \mathbf{I} the identity tensor, to describe passive Brownian motion over a planar surface with diffusion coefficient $D_0 = k_B T / \zeta_T$.

The partial case of passive Brownian diffusion taking place in a periodic surface potential is described by eq. (3) with vanishing self-propulsion, $\mathbf{v} = 0$:

$$\dot{\mathbf{x}}_c(t) = -\zeta_T^{-1} \nabla U(\mathbf{x}_c(t)) + \sqrt{2D_0} \boldsymbol{\xi}_T(t), \quad (4)$$

where the subscript ‘c’ stands for *crystalline* surface. The corresponding MSD, $\Delta R_{0,c}^2(t) = \langle |\mathbf{x}_c(t) - \mathbf{x}_c(0)|^2 \rangle$, is well approximated by a simple exponential memory [56, 57], which manifests itself in the velocity autocorrelation function (VACF) as

$$Z_{0,c}(t) := \frac{1}{4} \frac{d^2}{dt^2} \Delta R_{0,c}^2(t) = D_0 \delta(t-0^+) - \frac{\Delta D_c}{\tau_c} e^{-t/\tau_c}. \quad (5)$$

Here, τ_c is the longest relaxation time of the process and $\Delta D_c > 0$ describes the reduction of the long-time diffusivity due to the presence of the periodic surface relative to the planar case. This ansatz for the VACF corresponds to keeping only the largest non-zero eigenvalue of the Smoluchowski operator [58]. For the MSD, one readily calculates:

$$\Delta R_{0,c}^2(t) = 4 \int_0^t (t-s) Z_{0,c}(s) ds = 4(D_0 - \Delta D_c)t - 4\Delta D_c \tau_c (e^{-t/\tau_c} - 1). \quad (6)$$

It describes a simple crossover from free, unconfined diffusion with $D_0 = k_B T / \zeta_T$ at short times ($t \ll \tau_c$) to diffusion at long times with a reduced diffusion constant $D_{0,c} = D_0 - \Delta D_c \leq D_0$ for $t \gg \tau_c$. The crossover timescale τ_c describes the time after which the particle has explored a single potential minimum. Its inverse, τ_c^{-1} , may be interpreted as the attempt rate for escaping from the potential well [58, 59].

Next, we combine this result for passive motion in a periodic potential with active motion under the assumption that the diffusive motion in the potential be independent of the direction of the propulsion velocity. More precisely, we require that $\mathbf{x}_c(t)$ and $\mathbf{v}(t)$ are decorrelated on the scale of τ_c , noting that merely the increment $\boldsymbol{\xi}_T(t)$ is strictly independent of $\mathbf{v}(t)$. Then, the autocorrelation of the propulsion velocity is simply added to the VACF for passive diffusion,

$$Z_{a,c}(t) = Z_{0,c}(t) + \frac{1}{2} \langle \mathbf{v}(t) \cdot \mathbf{v}(0) \rangle. \quad (7)$$

Rotational diffusion of the cap orientation determines the propulsion velocity vector $\mathbf{v}(t)$ projected onto the surface plane. Neglecting the small gravitational torque on the present Janus particles (see also section 4.3), it follows that

$$\langle \mathbf{v}(t) \rangle = 0, \quad \langle \mathbf{v}(t) \cdot \mathbf{v}(0) \rangle = v^2 e^{-t/\tau_{\text{rot}}}, \quad (8)$$

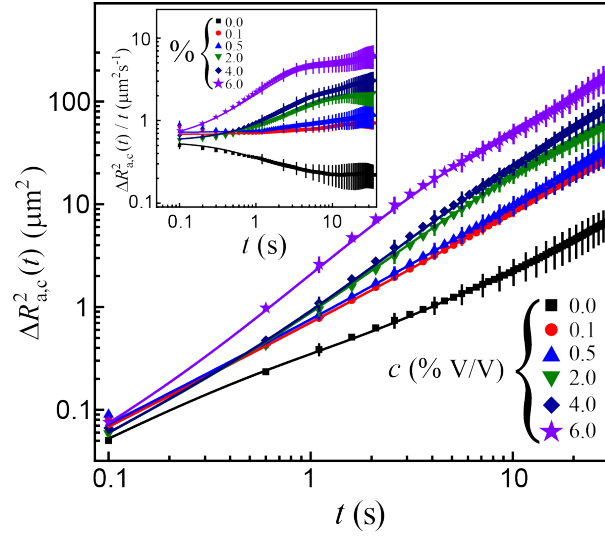


Figure 4. MSDs of the active particles moving atop the crystalline surface for six H_2O_2 concentrations % (v/v). The solid lines are fits to eq. (2). Inset: rectification of the same data by plotting $\Delta R_{a,c}^2(t)/t$ vs. t

with τ_{rot} the persistence time of the orientation; for free three-dimensional rotation $\tau_{\text{rot}} = (2D_{\text{rot}})^{-1}$. With this, the MSD of an active particle moving atop a crystalline surface follows from eqs. (5) and (7), again by integration:

$$\Delta R_{a,c}^2(t) = 4(D_0 - \Delta D_c + \frac{1}{2}v^2\tau_{\text{rot}})t - 4\Delta D_c\tau_c(e^{-t/\tau_c} - 1) + 2v^2\tau_{\text{rot}}^2(e^{-t/\tau_{\text{rot}}} - 1). \quad (9)$$

In section 4.3, this prediction will be checked against simulations.

4.2. Experiment

Figure 4 shows the averaged MSD data of Janus particles being actively propelled atop the crystalline surface for six H_2O_2 concentrations. As expected, increasing the H_2O_2 concentration leads to higher observed propulsion speeds and higher long-time diffusion. The latter can be directly inferred from the rectification $\Delta R_{a,c}^2(t)/t$ displayed in the inset of fig. 4. The data suggest further a monotonic dependence on time, either decreasing or increasing depending on the concentration of fuel, which we interpret as a competition of the suppression of diffusivity due to the potential landscape with the enhancement due to active motion.

Fitting eq. (9) to the experimental MSD data would, in principle, provide an estimate for the parameters ΔD_c , v , τ_c , τ_{rot} . Following this approach, it turned out all of the parameters depend on the H_2O_2 concentration. Specifically, fixing the values of v and τ_{rot} to those from the experiments with the planar surface does not produce satisfying fits. Further, the four-parameter fits suggest similar values for τ_c and τ_{rot} , which motivated us to merge both timescales into a single parameter, τ . This is consistent with the absence of any minimum or maximum at intermediate lag times in the data for $\Delta R_{a,c}^2(t)/t$, which would be supported by eq. (9). However, $\tau_c \approx \tau_{\text{rot}}$ implies that the parameters ΔD_c and v are no longer independent, merely the combination $\Delta D = \Delta D_c - v^2\tau/2$ can be obtained. Thus, eq. (9) reduces to a simplistic, effective model of the MSD of a self-propelled particle atop a periodic surface,

$$\Delta R_{a,c}^2(t) \approx 4D_{a,c}t + 4(D_{a,c} - D_0)\tau(e^{-t/\tau} - 1). \quad (10)$$

By construction, this result has the same form as eqs. (2) and (6), but the interpretation of the parameters is different in each case. For long times ($t \gg \tau_c, \tau_{\text{rot}}$), the MSD increases linearly, and

c (%v/v)	D_0 ($\mu\text{m}^2/\text{s}$)	$D_{\text{a,c}}$ ($\mu\text{m}^2/\text{s}$)	τ (s)
0	0.14 ± 0.01	0.05 ± 0.01	0.4 ± 0.2
0.1	0.17 ± 0.03	0.25 ± 0.03	6.3 ± 2.9
0.5	0.18 ± 0.02	0.29 ± 0.02	5.4 ± 2.2
2	0.14 ± 0.02	0.56 ± 0.02	2.3 ± 0.4
4	0.14 ± 0.03	0.8 ± 0.5	3.2 ± 0.1
6	0.14 ± 0.04	1.5 ± 0.4	1.5 ± 0.4

Table II. Parameter estimates from fitting eq. (10) to the MSD data shown in fig. 4. D_0 is the Brownian diffusion coefficient at short times, $D_{\text{a,c}}$ is the long-time diffusion coefficient of the self-propelled particle moving atop the crystalline surface, and $\tau \approx \tau_{\text{c}} \approx \tau_{\text{rot}}$ is a single crossover timescale.

the combination $D_{\text{a,c}} := D_0 - \Delta D_{\text{c}} + v^2\tau/2$ is the long-time diffusion coefficient on the crystalline surface.

We used eq. (10) to fit the MSD data with D_0 , $D_{\text{a,c}}$, and τ as free parameters. The results obtained for each concentration are given in table II and the fits shown as solid curves in fig. 4 provide a consistent description of the data. The enhancement of the long-time diffusivity $D_{\text{a,c}}$ with increasing H_2O_2 concentration is much less pronounced compared to the case of a planar surface ($D_{\text{a,p}}$ in table I), which is a direct consequence of the trapping potential. We again observe a slight variability of D_0 and a strong dependence of τ on the H_2O_2 concentration. We note that the MSD for $c = 0.1\%$ seems to deviate from the overall trend, and we exclude this data set from the remaining discussion.

4.3. Simulation of Langevin equations

As an independent check of the above approximate predictions and to gain further insight, we finally proceed to a refined theoretical model that explicitly includes both the translational and rotational degrees of freedom. The over-damped dynamics of an active bottom-heavy microswimmer [60] sedimenting due to gravity onto an HCP monolayer can effectively be described by Langevin equations for the projected position $\mathbf{x} = (x, y)$ and the orientation $\mathbf{u} = (u_x, u_y, u_z)$ [61, 62]:

$$\dot{\mathbf{x}}(t) = v_0 \mathbf{u}_{\parallel} - \zeta_{\text{T}}^{-1} \nabla U(\mathbf{x}(t)) + \sqrt{2D_{\text{T}}} \boldsymbol{\xi}_{\text{T}}(t), \quad (11)$$

$$\dot{\mathbf{u}}(t) = \left[\zeta_{\text{R}}^{-1} \mathbf{T} + \sqrt{2D_{\text{R}}} \boldsymbol{\xi}_{\text{R}}(t) \right] \times \mathbf{u} - 2D_{\text{R}} \mathbf{u}, \quad (12)$$

where Itô's interpretation of the white noise is adopted for the second equation. The first equation describes translational motion parallel to the surface and simply reproduces eq. (3), where we specify the propulsion term as $\mathbf{v} = v_0 \mathbf{u}_{\parallel}$. Here, v_0 is the propulsion strength and $\mathbf{u}_{\parallel} := (u_x, u_y)$ is the orthogonal projection of the three-dimensional unit vector \mathbf{u} onto the xy -plane. The second equation governs the cap orientation \mathbf{u} of the Janus particle, in which $\mathbf{T} = m r_0 \mathbf{u} \times \mathbf{g}$ is the gravitational torque with $m = V_{\text{SiO}_2} \rho_{\text{SiO}_2} + V_{\text{Pt}} \rho_{\text{Pt}}$ the mass of the particle and r_0 the displacement of the center of mass from the center of the sphere due to the heavy cap; for the Janus particle used in the present experiments, $r_0 \approx 0.02a$. The strength of thermal fluctuations is determined by $D_{\text{T}} = k_{\text{B}}T/\zeta_{\text{T}}$ and $D_{\text{R}} = k_{\text{B}}T/\zeta_{\text{R}}$, the diffusivities of the translational and rotational motions, respectively, with $\boldsymbol{\xi}_{\text{T}}$ and $\boldsymbol{\xi}_{\text{R}}$ being independent Gaussian white noises having zero mean and unit covariance. The effective substrate potential $U(x, y) = \Delta m g z(x, y)$ arises from the buoyancy-corrected gravitational force $\Delta m g$ on the Janus particle with its height given by the landscape $z(x, y)$. In this effectively two-dimensional representation, the center of the Janus particle is constrained to the surface $z = z(x, y)$, which is created by the HCP colloidal monolayer and is composed of the upper non-intersecting segments of spheres,

$$z(x, y) = \sqrt{(h + a)^2 - (x - x_i)^2 - (y - y_i)^2}, \quad (13)$$

located at the centers (x_i, y_i) of the monolayer particles, which form a hexagonal lattice of lattice constant $d = 2a = 2 \mu\text{m}$, see fig. 2(a). For the sphere radius, we use $h + a \approx 2.3 \mu\text{m}$ as estimated

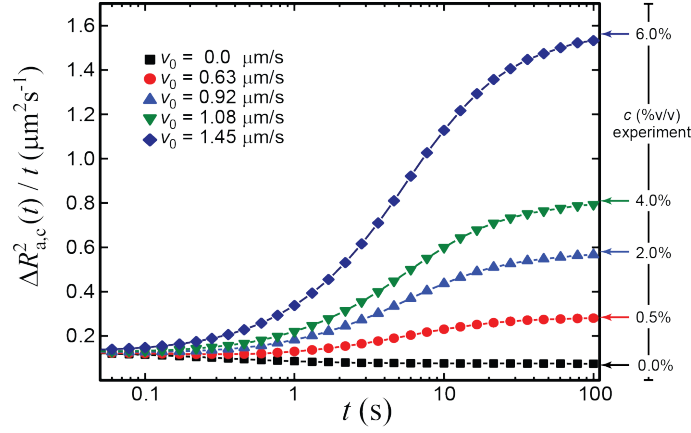


Figure 5. The MSDs obtained from simulations (markers) for different values of v_0 for $D_T = 0.13 \mu\text{m}^2/\text{s}$, $D_R = 0.15 \text{s}^{-1}$ and the corresponding fits (solid lines) of eq. (10); see also table III. In the simulations, v_0 is adjusted such that the experimental long-time diffusion coefficients $D_{a,c}$ (arrows) for the different H_2O_2 concentrations are approximately recovered.

in section 2.4, see also fig. 2(d).

The presence of the surface also modifies the rotational hydrodynamic friction. With the above value of the elevation h , we estimate for the rotational diffusion constants, which are distinct for rotations parallel and perpendicular to the surface [15, 63]:

$$\frac{D_R^\parallel}{D_R^{\text{St}}} \approx 1 - \frac{1}{8} \left(\frac{a}{h}\right)^3, \quad \frac{D_R^\perp}{D_R^{\text{St}}} \approx 1 - \frac{5}{16} \left(\frac{a}{h}\right)^3, \quad (14)$$

where $D_R^{\text{St}} = k_B T / 8\eta\pi a^3$. For the sake of simplicity and since we are only interested in the correlation $\langle \mathbf{u}(t) \cdot \mathbf{u}(0) \rangle$, we further use the average rotational diffusion constant

$$D_R := \frac{1}{3} \left(D_R^\parallel + 2D_R^\perp \right) = \left[1 - \frac{1}{4} \left(\frac{a}{h}\right)^3 \right] D_R^{\text{St}}, \quad (15)$$

such that $D_R \approx 0.15 \text{s}^{-1}$ and $\tau_{\text{rot}} = (2D_R)^{-1} \approx 3.3 \text{s}$. With this, the model eqs. (11) and (12) are fully specified with v_0 as a control parameter and is solved numerically with the standard Euler-Maruyama scheme. We have validated the numerical scheme for the planar case ($U = 0$) by comparing simulated MSDs with the exact solution, eq. (2), for this case.

First of all we note that eq. (12) for the orientational dynamics is decoupled from the translational motion, eq. (11). Yet, it remains analytically challenging due to the gravitational torque term, $\mathbf{T} \neq 0$. The numerical results suggest that the dynamics of the orientation is well approximated by the free solution $\langle \mathbf{u}(t) \rangle = 0$ and $\langle \mathbf{u}(t) \cdot \mathbf{u}(0) \rangle = e^{-2D_R t}$ and therefore $\tau_{\text{rot}} = (2D_R)^{-1}$. Thus, the problem described by eqs. (11) and (12) becomes equivalent to the model defined by eq. (3) with the velocity correlation prescribed via eq. (8). Note that although the orientation of the particle is three-dimensional, the translational motion of the particle is essentially restricted to the horizontal plane. As a result, for the mean-square velocity entering eq. (8) we have $v^2 := \langle (v_0 \mathbf{u}_\parallel)^2 \rangle = 2v_0^2/3$. The latter step tacitly assumes that all orientations of \mathbf{v} are equally probable, which is fulfilled under the approximation of free rotational diffusion.

Simulations of the active motion of the Janus particle in the hexagonal landscape, eqs. (11) and (12), were performed for different values of v_0 with all other parameters fixed to their values as mentioned above. The obtained MSDs shown in fig. 5 capture the trends of the experimental data (fig. 4) semi-quantitatively and reproduce the long-time diffusion coefficients for propulsion velocities $v = \sqrt{2/3}v_0$ similar to the experimental values.

Finally, the numerical solutions permit a number of insights into the analytic predictions for the MSD. First, simulations addressing the passive motion above the crystalline surface show

v_0 ($\mu\text{m/s}$)	v ($\mu\text{m/s}$)	$D_{a,c}$ ($\mu\text{m}^2/\text{s}$)	τ (s)
0	0	0.07	0.2
0.63	0.51	0.29	5.2
0.92	0.75	0.58	3.2
1.08	0.88	0.81	3.2
1.45	1.18	1.57	3.2

Table III. Parameters $D_{a,c}$ and τ obtained from fitting eq. (10) to the simulated MSDs (fig. 5) for different propulsion velocities v_0 , keeping $D_T = D_0 = 0.13 \mu\text{m}^2/\text{s}$ and $D_R = 0.15 \text{s}^{-1}$ fixed. For comparison with experiment, the projected propulsion velocity $v = \sqrt{2/3}v_0$ is quoted as well.

that eq. (6) is a very good approximation for the experimental regime investigated here. With $D_T = 0.13 \mu\text{m}^2/\text{s}$ and $D_R = 0.15 \text{s}^{-1}$, excellent quantitative agreement between the simulated MSD and the theory is found for the parameters $\tau_c \approx 0.18 \text{s}$ and $\Delta D_c \approx 0.055 \mu\text{m}^2/\text{s}$. Second, simulations of active motion above the crystalline surface indicate that the approximation eq. (9) does not work universally. For the considered range of propulsion velocities v_0 , the simulated MSDs are significantly overestimated by eq. (9) if ΔD_c and τ_c are fixed to their values for passive motion ($v_0 = 0$). For the cases where $\Delta R_{a,c}(t)/t$ is monotonic in t , it is, however, possible to obtain good descriptions if we allow ΔD_c and τ_c to depend on the activity, v_0 , and estimate them by the fit for each value of v_0 . Third, for these monotonic cases we have found that eq. (10) is a good approximation to the MSD, see fig. 5 and table III. On one hand, it provides less flexibility because it contains fewer parameters, in particular it allows for only a single crossover. On the other hand, this is sufficient to capture the full time dependence in these cases and the formula is simpler to handle than eq. (9). Note that for high H_2O_2 concentrations, when $D_{a,c}$ is larger than D_0 , the crossover time saturates, $\tau \approx \tau_{\text{rot}}$. For low H_2O_2 concentrations, when $D_{a,c} \simeq D_0$, τ may differ from τ_R quite significantly.

5. Conclusions

We have studied the problem of propulsion of an active colloidal particle above a crystalline surface by a combination of experiment, theory, and numerical simulations. The experimental system consists of catalytically driven colloidal Janus spheres sedimenting due to gravity on top of a periodic substrate. The strength of self-propulsion is controlled by changing the concentration of the chemical fuel, H_2O_2 . Due to a relatively heavy cap, the center of mass of the nearly spherical active particle is slightly displaced from its center, which makes it bottom heavy. The substrate is realized by a HCP colloidal monolayer made of passive stationary colloidal particles of similar size and material. We have investigated the mean-square displacement of the Janus particle and extracted the parameters characterizing different regimes of motion. In particular, we looked at the long-time diffusion coefficient, how it changes relative to the free diffusivity and how it develops from the Brownian motion at short timescales.

We have considered two limiting cases, which permit comparably simple interpretations, and finally studied their interplay. First, we have focused on the active propulsion above a planar surface, which shows an enhanced long-time diffusion constant and is in agreement with previously known results. Fitting the full time dependence of the MSDs provides additional details on how activity modifies the rotational diffusion. Second, we have investigated the case of passive diffusion above a crystalline surface, which plays the role of a trapping potential and results in the suppression of the particle diffusivity. Third, we have studied the interplay of these two factors, which have opposite effects on the diffusion constant. We show that depending on the strength of the activity relative to the strength of the trapping potential, the long-time diffusion constant can be either lower (weak activity) or higher (strong activity) relative to the free diffusion. In all instances studied, the diffusion constant of an active particle remains larger than that of a passive particle.

The analytical theory is based on a simplified overdamped Langevin equation, eq. (3). Based on the fact that the gravitational torque of the particle is weak, we reduce the problem to the case of a particle whose orientation is subject to free diffusion and suggest a theoretical formula that describes the mean-square displacement and involves two generally distinct timescales to describe the twofold crossover from free to active diffusion due to (i) the periodic trapping potential and (ii) rotational diffusion. Further, we show that the present experimental data display a simple crossover involving only one timescale. Numerical simulations of the full Langevin model, eqs. (11) and (12), explicitly addressing both the translational and orientational degrees of freedom, confirm the expressions for the MSD in the partial cases of active motion above a planar surface [eq. (2)] and for the case of passive motion above the crystalline surface [eq. (6)]. For the general case, the suggested analytical formula, eq. (9), is shown to serve as an approximation with only semi-quantitative agreement with the numerical model.

Finally, we note that our analysis of the experiment does not depend on details of the propulsion mechanism and on the particular realization of the confining potential. Therefore, we expect that our findings apply equally to a broad class of microswimmers moving in a periodic landscape.

Acknowledgements

This work was supported in part by the Deutsche Forschungsgemeinschaft (DFG) as part of the project SPP 1726 (microswimmers, FI 1966/1-1) and in part by the State of Arizona Technology and Research Initiative Fund (TRIF), administered by the Arizona Board of Regents.

References

- [1] E. Lauga and T. R. Powers, “The hydrodynamics of swimming microorganisms,” *Rep. Prog. Phys.* **72**, 096601 (2009).
- [2] I. S. Aranson, “Active colloids,” *Physics – Uspekhi* **56**, 79 (2013).
- [3] C. Bechinger, R. Di Leonardo, H. Löwen, C. Reichhardt, G. Volpe, and G. Volpe, “Active particles in complex and crowded environments,” *Rev. Mod. Phys.* **88**, 045006 (2016).
- [4] A. Zöttl and H. Stark, “Emergent behavior in active colloids,” *J. Phys.: Condens. Matter* **28**, 253001 (2016).
- [5] H. Löwen, “Colloidal soft matter under external control,” *J. Phys.: Condens. Matter* **13**, R415 (2001).
- [6] A. Ghosh and P. Fischer, “Controlled propulsion of artificial magnetic nanostructured propellers,” *Nano Lett.* **9**, 2243 (2009).
- [7] J. Dobnikar, A. Snezhko, and A. Yethiraj, “Emergent colloidal dynamics in electromagnetic fields,” *Soft Matter* **9**, 3693 (2013).
- [8] P. Tierno, “Recent advances in anisotropic magnetic colloids: realization, assembly and applications,” *Phys. Chem. Chem. Phys.* **16**, 23515 (2014).
- [9] S. H. L. Klapp, “Collective dynamics of dipolar and multipolar colloids: From passive to active systems,” *Curr. Opinion Colloid & Interface Sci.* **21**, 76 (2016).
- [10] W. F. Paxton, K. C. Kistler, C. C. Olmeda, A. Sen, S. K. St. Angelo, Y. Cao, T. E. Mallouk, P. E. Lammert, and V. H. Crespi, “Catalytic nanomotors: autonomous movement of striped nanorods,” *J. Am. Chem. Soc.* **126**, 13424 (2004).
- [11] J. R. Howse, R. A. Jones, A. J. Ryan, T. Gough, R. Vafabakhsh, and R. Golestanian, “Self-motile colloidal particles: from directed propulsion to random walk,” *Phys. Rev. Lett.* **99**, 048102 (2007).
- [12] H.-R. Jiang, N. Yoshinaga, and M. Sano, “Active motion of a Janus particle by self-thermophoresis in a defocused laser beam,” *Phys. Rev. Lett.* **105**, 268302 (2010).
- [13] I. Buttinoni, G. Volpe, F. Kümmel, G. Volpe, and C. Bechinger, “Active Brownian motion tunable by light,” *J. Phys.: Condens. Matter* **24**, 284129 (2012).
- [14] K. Kroy, D. Chakraborty, and F. Cichos, “Hot microswimmers,” *Eur. Phys. J. Special Topics* **225**, 2207 (2016).
- [15] J. Happel and H. Brenner, *Low Reynolds number hydrodynamics: with special applications to particulate media*, Vol. 1 (Springer Science & Business Media, 2012).
- [16] J. Palacci, S. Sacanna, A. P. Steinberg, D. J. Pine, and P. M. Chaikin, “Living crystals of light-activated colloidal surfers,” *Science* **339**, 936 (2013).

- [17] A. Zöttl and H. Stark, “Hydrodynamics determines collective motion and phase behavior of active colloids in quasi-two-dimensional confinement,” *Phys. Rev. Lett.* **112**, 118101 (2014).
- [18] J. Schwarz-Linek, C. Valeriani, A. Cacciuto, M. Cates, D. Marenduzzo, A. Morozov, and W. Poon, “Phase separation and rotor self-assembly in active particle suspensions,” *Proc. Natl. Acad. Sci.* **109**, 4052 (2012).
- [19] X. Ma, K. Hahn, and S. Sanchez, “Catalytic mesoporous Janus nanomotors for active cargo delivery,” *J. Am. Chem. Soc.* **137**, 4976 (2015).
- [20] S. Das, A. Garg, A. I. Campbell, J. Howse, A. Sen, D. Velegol, R. Golestanian, and S. J. Ebbens, “Boundaries can steer active Janus spheres,” *Nature Commun.* **6** (2015).
- [21] W. Uspal, M. N. Popescu, S. Dietrich, and M. Tasinkevych, “Self-propulsion of a catalytically active particle near a planar wall: from reflection to sliding and hovering,” *Soft Matter* **11**, 434 (2015).
- [22] J. Simmchen, J. Katuri, W. E. Uspal, M. N. Popescu, M. Tasinkevych, and S. Sánchez, “Topographical pathways guide chemical microswimmers,” *Nature Commun.* **7** (2016).
- [23] A. Nourhani, S. J. Ebbens, J. G. Gibbs, and P. E. Lammert, “Spiral diffusion of rotating self-propellers with stochastic perturbation,” *Phys. Rev. E* **94**, 030601 (2016).
- [24] P. Malgaretti, M. Popescu, and S. Dietrich, “Active colloids at fluid interfaces,” *Soft Matter* **12**, 4007 (2016).
- [25] K. Schaar, A. Zöttl, and H. Stark, “Detention times of microswimmers close to surfaces: Influence of hydrodynamic interactions and noise,” *Phys. Rev. Lett.* **115**, 038101 (2015).
- [26] M. Evstigneev, O. Zvyagolskaya, S. Bleil, R. Eichhorn, C. Bechinger, and P. Reimann, “Diffusion of colloidal particles in a tilted periodic potential: Theory versus experiment,” *Phys. Rev. E* **77**, 041107 (2008).
- [27] A. V. Straube and P. Tierno, “Synchronous vs. asynchronous transport of a paramagnetic particle in a modulated ratchet potential,” *EPL (EuroPhys. Lett.)* **103**, 28001 (2013).
- [28] M. P. Juniper, A. V. Straube, D. G. Aarts, and R. P. Dullens, “Colloidal particles driven across periodic optical-potential-energy landscapes,” *Phys. Rev. E* **93**, 012608 (2016).
- [29] M. Pelton, K. Ladavac, and D. G. Grier, “Transport and fractionation in periodic potential-energy landscapes,” *Phys. Rev. E* **70**, 031108 (2004).
- [30] M. Kim, S. M. Anthony, and S. Granick, “Activated surface diffusion in a simple colloid system,” *Phys. Rev. Lett.* **102**, 178303 (2009).
- [31] X.-g. Ma, P.-Y. Lai, and P. Tong, “Colloidal diffusion over a periodic energy landscape,” *Soft Matter* **9**, 8826 (2013).
- [32] X.-g. Ma, P.-Y. Lai, B. J. Ackerson, and P. Tong, “Colloidal transport and diffusion over a tilted periodic potential: dynamics of individual particles,” *Soft Matter* **11**, 1182 (2015).
- [33] Y. Su, P.-Y. Lai, B. J. Ackerson, X. Cao, Y. Han, and P. Tong, “Colloidal diffusion over a quasicrystalline-patterned surface,” *J. Chem. Phys.* **146**, 214903 (2017).
- [34] P. Tierno, F. Sagués, T. H. Johansen, and I. M. Sokolov, “Antipersistent random walk in a two state flashing magnetic potential,” *Phys. Rev. Lett.* **109**, 070601 (2012).
- [35] F. Martinez-Pedrero, H. Massana-Cid, T. Ziegler, T. H. Johansen, A. V. Straube, and P. Tierno, “Bidirectional particle transport and size selective sorting of Brownian particles in a flashing spatially periodic energy landscape,” *Phys. Chem. Chem. Phys.* **18**, 26353 (2016).
- [36] P. Tierno and M. R. Shaebani, “Enhanced diffusion and anomalous transport of magnetic colloids driven above a two-state flashing potential,” *Soft Matter* **12**, 3398 (2016).
- [37] T. Brazda, C. Joly, and C. Bechinger, “Experimental observation of Shapero-steps in colloidal monolayers driven across time-dependent substrate potentials,” *Soft Matter* **13**, 4024 (2017).
- [38] F. Evers, C. Zunke, R. D. Hanes, J. Bewerunge, I. Ladadwa, A. Heuer, and S. U. Egelhaaf, “Particle dynamics in two-dimensional random-energy landscapes: Experiments and simulations,” *Phys. Rev. E* **88**, 022125 (2013).
- [39] Y. Su, X.-g. Ma, P.-Y. Lai, and P. Tong, “Colloidal diffusion over a quenched two-dimensional random potential,” *Soft Matter* (2017), 10.1039/C7SM01056G.
- [40] T. O. E. Skinner, S. K. Schnyder, D. G. A. L. Aarts, J. Horbach, and R. P. A. Dullens, “Localization dynamics of fluids in random confinement,” *Phys. Rev. Lett.* **111**, 128301 (2013).
- [41] S. K. Schnyder, M. Spanner, F. Höfling, T. Franosch, and J. Horbach, “Rounding of the localization transition in model porous media,” *Soft Matter* **11**, 701 (2015).
- [42] S. Leitmann and T. Franosch, “Time-dependent fluctuations and superdiffusivity in the driven lattice Lorentz gas,” *Phys. Rev. Lett.* **118**, 018001 (2017).
- [43] J. Palacci, C. Cottin-Bizonne, C. Ybert, and L. Bocquet, “Sedimentation and effective temperature of active colloidal suspensions,” *Phys. Rev. Lett.* **105**, 088304 (2010).

- [44] A. Geiseler, P. Hänggi, and G. Schmid, “Kramers escape of a self-propelled particle,” *Eur. Phys. J. B* **89**, 175 (2016).
- [45] A. Pototsky and H. Stark, “Active Brownian particles in two-dimensional traps,” *EPL (Europhys. Lett.)* **98**, 50004 (2012).
- [46] W. Schirmacher, B. Fuchs, F. Höfling, and T. Franosch, “Anomalous magnetotransport in disordered structures: Classical edge-state percolation,” *Phys. Rev. Lett.* **115**, 240602 (2015).
- [47] M. Zeitz, K. Wolff, and H. Stark, “Active Brownian particles moving in a random Lorentz gas,” *Eur. Phys. J. E* **40**, 23 (2017).
- [48] W. Gao, A. Pei, X. Feng, C. Hennessy, and J. Wang, “Organized self-assembly of Janus micromotors with hydrophobic hemispheres,” *J. Am. Chem. Soc.* **135**, 998 (2013).
- [49] U. Choudhury, L. Soler, J. G. Gibbs, S. Sanchez, and P. Fischer, “Surface roughness-induced speed increase for active Janus micromotors,” *Chem. Commun.* **51**, 8660 (2015).
- [50] J. Gibbs and Y.-P. Zhao, “Design and characterization of rotational multicomponent catalytic nanomotors,” *Small* **5**, 2304 (2009).
- [51] M. Bardosova, M. E. Pemble, I. M. Povey, and R. H. Tredgold, “The Langmuir-Blodgett approach to making colloidal photonic crystals from silica spheres,” *Adv. Mater.* **22**, 3104 (2010).
- [52] M. Szekeres, O. Kamalin, P. Grobet, R. Schoonheydt, K. Wostyn, K. Clays, A. Persoons, and I. Dékány, “Two-dimensional ordering of Stöber silica particles at the air/water interface,” *Colloids and Surfaces A: Physicochemical and Engineering Aspects* **227**, 77 (2003).
- [53] A. I. Campbell and S. J. Ebbens, “Gravitaxis in spherical Janus swimming devices,” *Langmuir* **29**, 14066 (2013).
- [54] A. J. Goldman, R. G. Cox, and H. Brenner, “Slow viscous motion of a sphere parallel to a plane wall — I Motion through a quiescent fluid,” *Chem. Eng. Sci.* **22**, 637 (1967).
- [55] Y. He, J. Wu, and Y. Zhao, “Designing catalytic nanomotors by dynamic shadowing growth,” *Nano Lett.* **7**, 1369 (2007).
- [56] P. Fulde, L. Pietronero, W. R. Schneider, and S. Strässler, “Problem of Brownian motion in a periodic potential,” *Phys. Rev. Lett.* **35**, 1776 (1975).
- [57] H. Risken and H. D. Vollmer, “Correlation functions for the diffusive motion of particles in a periodic potential,” *Z. Phys. B: Condens. Matter* **31**, 209 (1978).
- [58] R. Festa and E. G. d’Aglano, “Diffusion coefficient for a Brownian particle in a periodic field of force: I. Large friction limit,” *Physica A* **90**, 229 (1978).
- [59] H. A. Kramers, “Brownian motion in a field of force and the diffusion model of chemical reactions,” *Physica* **7**, 284 (1940).
- [60] K. Wolff, A. M. Hahn, and H. Stark, “Sedimentation and polar order of active bottom-heavy particles,” *Eur. Phys. J. E* **36**, 43 (2013).
- [61] B. Øksendal, *Stochastic Differential Equations* (Springer, Berlin Heidelberg, 2003).
- [62] S. Leitmann, F. Höfling, and T. Franosch, “Dynamically crowded solutions of infinitely thin Brownian needles,” *Phys. Rev. E* **96**, 012118 (2017).
- [63] J. Leach, H. Mushfique, S. Keen, R. Di Leonardo, G. Ruocco, J. M. Cooper, and M. J. Padgett, “Comparison of Faxén’s correction for a microsphere translating or rotating near a surface,” *Phys. Rev. E* **79**, 026301 (2009).